Reentrant phenomenon in the diffuse ferroelectric $BaSn_{0.15}Ti_{0.85}O_3$: Local structural insights and first-order reversal curves study

Akash Surampalli,[1] Ramon Egli,[2] Deepak Prajapat,[1] Carlo Meneghini,[3] and V. Raghavendra Reddy[1,*]

[1]*UGC-DAE Consortium for Scientific Research, University Campus, Khandwa Road, Indore 452001, India*

[2]*Central Institute for Meteorology and Geodynamics (ZAMG), 1190 Vienna, Austria*

[3]*Dipartimento di Scienze, Universita di Roma Tre, I-00146 Roma, Italy*

(Received 27 July 2021; revised 3 November 2021; accepted 4 November 2021; published 23 November 2021)

From the phase diagram proposed by Lei *et al.* [J. Appl. Phys. **101**, 084105 (2007)], $BaSn_{0.15}Ti_{0.85}O_3$ is chosen. It also exhibits a diffuse phase transition between cubic and rhombohedral (*C*-*R*) near room temperature. Dielectric analysis confirms a phase transition near room temperature ($T_C \approx 290$ K). In addition, frequency dispersion in the dielectric constant, concomitantly, a loss peak is observed at low temperatures ($T < T_C$). Furthermore, in the similar temperature range, a decrease in remanent polarization is seen upon lowering the temperature. All of these findings point to a reentering phenomenon in the system. First-order reversal curves $P(E_r, E)$ are measured at different temperatures and analyzed to better understand the system's interactions and polarization evolution. It was found that the relaxor nature present in the system is responsible for the reentrant behavior. Local probe techniques such as x-ray absorption near-edge spectroscopy, Raman spectroscopy, and Mössbauer spectroscopy are employed to investigate the local environment changes that are associated with the reentrant behavior. A simple ferroelectric exchange model explaining the low-temperature reentrant behavior is presented from these results.

DOI: 10.1103/PhysRevB.104.184114

I. INTRODUCTION

The ferroelectric (FE) transition with a frequency-independent broad dielectric peak as a function of temperature is usually denoted as the diffused phase transition (DPT) in order to distinguish it from the relaxor one [1–3]. Relaxors are usually associated with frequency dependency in their dielectric response, and they are made of polar regions of microscopic size [usually in the nanometer range, i.e., polar nanoregions (PNRs)] showing a different electric field response from the usual domainlike response as observed in FE materials.

The earliest models proposed for DPT systems are indistinguishable from relaxors, in which the smearing of a transition is explained in terms of statistical compositional fluctuations that occur among equivalent crystallographic sites due to doping [3]. Such fluctuations in composition lead to the distribution of local Curie temperatures $\langle T_C \rangle$ in the system, resulting in a broad temperature range of transition. The authors argued that different local and global symmetries have stringent consequences on their poling-depoling behavior and their low-temperature dielectric dispersion [3]. For instance, Setter *et al.* demonstrated experimentally that introducing disorder to lead-scandium-tantalate (PST, $PbSc_xTa_{1-x}O_3$) makes the ferroelectric transition go from sharp to diffuse [4].

On the other hand, it has been suggested that the mechanism of DPT involved in relaxors differs from those exhibited in FE materials [5]. Unlike FE, relaxors do not exhibit any phase transition across the dielectric maximum, and instead the DPT in relaxors is explained as an overlapping phenomenon of volume increase of polar microregions (which are manifested at high temperatures above the dielectric maximum temperature) and the freezing of dipoles [5]. Based on this idea, further models have been proposed taking analogies with spin-glass models to explain the relaxor behavior [6]. Further, experimental evidence of PNR and nonlinear dielectric responses as predicted from these models has been found [7–9]. This led to characterizing relaxors as a separate class from FE. However, with the observation of soft-mode-like behavior and domainlike responses in the relaxors, the earliest interpretations of relaxors have been revived, and relaxors are defined as FE with multiple inhomogeneities [10].

Barium titanate ($BaTiO_3$, BTO) and its modified systems have been well studied for their intriguing physics and applicability [11–14]. In particular, the systems in which titanium was replaced with an isovalent atom exhibit dielectric and polarization responses that are different from FE systems. In the literature, the compositional phase diagrams of such systems are studied in detail. In particular, the phase diagram of $BaTi_{1-x}Sn_xO_3$ has been studied intensively due to its excellent properties, such as the electrocaloric effect [14–16]. With increasing Sn doping, the system exhibits a transformation from FE to relaxors showing diffuse ferroelectric phase transitions for intermediate compositions [16].

The system being investigated herein, i.e., the solid solution $BaTi_{1-x}Sn_xO_3$ for a particular composition ($x = 0.15$) exhibiting DPT, has been a subject of research in the past decade [11,12,15,17–20]. These past studies were usually focused on the phase segregation that exists in this compound,

*varimalla@yahoo.com; vrreddy@csr.res.in

and the existence of FE-like regions above $\langle T_C \rangle$. Xie *et al.* observed both staticlike and dynamiclike polar regions above $\langle T_C \rangle$, transforming to a long-range FE below $\langle T_C \rangle$ [19]. Similar observations were made by Shvartsman *et al.*, who argued that the phase transition occurring in $BaTi_{0.85}Sn_{0.15}O_3$ is different from the conventional FE transition [12]. Precursor polarlike regions that are responsible for transitions are seen above dielectric maxima (T_m), and the bulk transformation to FE is completed at a much lower temperature ($T < T_m$). However, in a later work published by Sanjay *et al.* that focused on a similar composition, it was conjectured that toward low temperature, the relaxor phase sets in coexisting with FE [11]. This is interpreted from the changes in polarization hysteresis curves in the electric-field-cooled conditions and reentrantlike behavior in remanent polarization variation with temperature.

There is no further consensus available on the above-mentioned aspects, and in general there have been very few explorations of the reentrant phenomenon in the context of FE materials as compared to their magnetic counterparts [21–23]. Reentrant phases are usually associated with a disordered phase that is followed by an ordered phase upon lowering the temperature. Such disorder is likely to occur by breaking the ordered state into a disordered state or by having different phases coexist at different scales [24]. Reentrant phenomena in ferroelectrics are distinguished in materials that reveal a typical sequence of phase transitions, viz., paraelectric-ferroelectric-relaxor upon lowering the temperature. These phase transitions are identified by a decrease in polarization, dispersion in the dielectric constant, and an associated loss peak, aging at low temperatures [25–28]. Investigating reentrant transitions in ferroelectrics is especially challenging since the properties that are associated with them can be explained with an external process, i.e., domain wall and domain responses. Hence, the idea that reentrant phases in ferroelectrics are associated with a thermodynamic phase transition is received with skepticism [26].

In view of this, in the present work we have taken the system $BaSn_{0.15}Ti_{0.85}O_3$ in which the properties associated with reentrant behavior are observed [11]. To understand the polarization evolution in the system, we have employed first-order reversal curves (FORC) to reveal subtle changes that are responsible for the reentrant behavior or to find out if such behavior exists. Along with it, x-ray absorption spectroscopy (XAS), Mössbauer spectroscopy, and Raman spectroscopy techniques are further employed to understand the structural changes occurring across this reentrant temperature. It may be noted that the combined use of such microscopic and macroscopic experimental techniques has revealed structural modifications associated with the relaxor behavior in BTO-based compounds in our recent work [29].

II. EXPERIMENTAL DETAILS

Polycrystalline 15% Sn-doped $BaTiO_3$ ($BaSn_{0.15}Ti_{0.85}O_3$) is prepared with a conventional solid-state sintering method starting from high-purity ($\geqslant$99.9%) oxide and carbonate precursors. X-ray diffraction measurements are carried out with the Brucker D8-Discover system equipped with Cu $K\alpha$ radiation and a LynxEye detector. Dielectric measurements were performed using a precision LCR meter E4980 and an in-house developed sample holder with a 1 V ac signal at different frequencies in the temperature range 50–300 K while cooling the sample. Temperature-dependent *P-E* hysteresis loops and first-order reversal curves (FORC) were measured using a Radiant Precision Premier II ferroelectric loop tracer using liquid nitrogen as cryogen in the temperature range of 80–350 K and placing the sample in a Delta-9023 chamber. Temperature-dependent Raman spectra were recorded with LabRam-HR800 in backscattering geometry equipped with a diode laser ($\lambda = 473$ nm) as an excitation source in the temperature range 80–325 K using a Linkam cryostat. Temperature-dependent Ti *K* edge x-ray absorption spectra (XAS) data were collected in transmission geometry at the ELETTRA (Trieste, Italy) 11.1R beamline [30]. Absorption spectra were measured in transmission geometry using Ti foil as a reference sample for energy calibration. The raw data were treated using standard procedures for normalization and extraction of the XAFS signal [31]. Temperature-dependent ^{119}Sn Mössbauer measurements are carried out in transmission mode using a standard PC-based Mössbauer spectrometer equipped with a WissEl velocity drive in constant acceleration mode and placing the sample in a Janis CCR system. The spectrometer is calibrated with natural iron, and the isomer shift values are reported with respect to SnO_2.

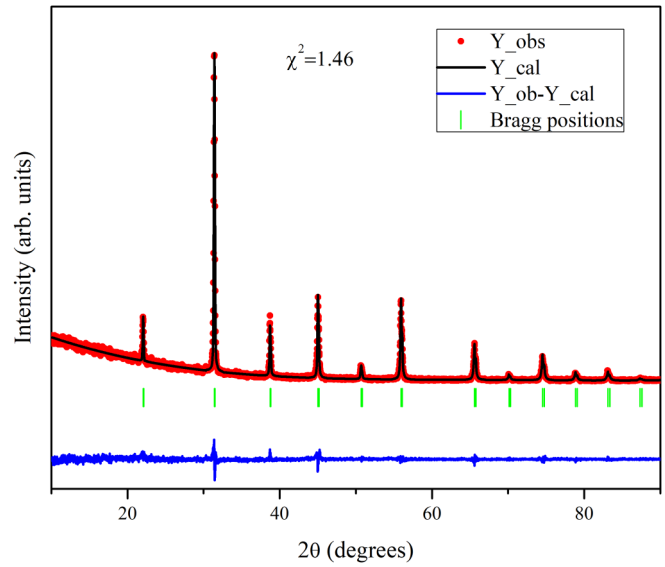

FIG. 1. Room-temperature x-ray diffraction pattern of $BaSn_{0.15}Ti_{0.85}O_3$ measured with $\lambda = 0.154$ nm radiation. The experimental data are profile-fitted with the FULLPROF [32] program.

III. RESULTS AND DISCUSSIONS

The x-ray powder diffraction data obtained at room temperature (shown in Fig. 1) reveal a $Pm\bar{3}m$ cubic symmetry consistent with the literature [16]. The χ^2 value is found to be well within the accepted range. The XRD data indicate the phase purity of the studied sample, and the results of all the measurements are discussed in the following sections.

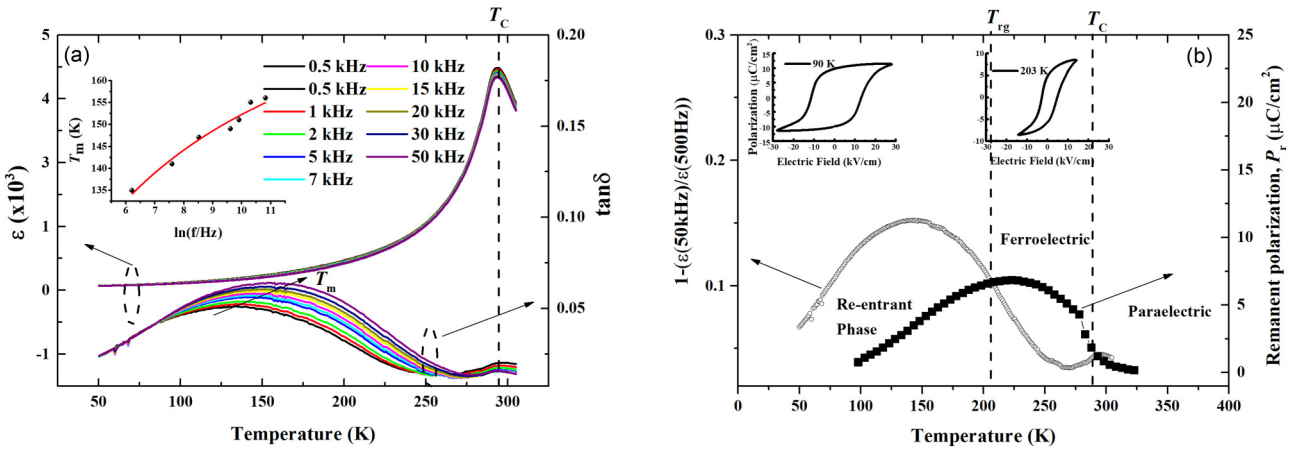

FIG. 2. (a) Temperature-dependent dielectric constant (ϵ) and tanδ of $BaSn_{0.15}Ti_{0.85}O_3$ at different frequencies. The inset shows the Vogel-Fulcher fit to the variation of T_m as a function of frequency. (b) Variation of $1-[\epsilon(50\text{ kHz})/\epsilon(500\text{ Hz})]$ as a function of temperature of $BaSn_{0.15}Ti_{0.85}O_3$ and remanent polarization, P_r vs temperature as obtained from PUND measurements, taken at an electric field of around 8 kV/cm. The inset shows the *P-E* loops at the indicated temperatures.

A. Temperature-dependent dielectric and electric polarization studies

The temperature-dependent dielectric constant (ϵ) and dielectric loss (tanδ) are shown in Fig. 2. Upon cooling, it can be seen from Fig. 2(a) that at around 290 K (T_C), a broad peak in the dielectric constant is seen, a characteristic of DPT, as well as a peak in the dielectric loss near the same temperature. This is a feature reminiscent of the paraelectric-ferroelectric transition (T_C). Upon further lowering the temperature, frequency dispersion in the dielectric constant becomes evident, and a steady increase in loss is seen with the frequency-dependent dispersive peak. The loss peaks roughly follow Vogel-Fulcher law, indicating the possible existence of dipolar freezing dynamics in the system. The frequency dispersion in ϵ, represented as $1-\frac{\epsilon_{50\,\text{kHz}}}{\epsilon_{500\,\text{kHz}}}$, shows a behavior similar to tanδ, as shown in Fig. 2(b). The frequency dispersion starts to appear above T_C, showing a local maxima around T_C. The relaxation around the dielectric maxima was already discussed by Shvartsman *et al.*, who demonstrated that relaxing polar entities manifested at high temperatures percolating to the ferroelectric state are responsible for this dispersion around the dielectric maxima [12]. This FE transition is accompanied by increasing dispersion upon further lowering the temperature, peaking at a specific temperature and starting to vanish below that. To investigate such behavior at low temperatures, electric polarization versus electric field (*P-E*) loop evolution with temperature and remanent polarization obtained from positive up and negative down (PUND) measurements are performed and are also shown in Fig. 2(b) comparing with the trend in dielectric dispersion in the system.

Apart from the dispersion in the dielectric constant, remanent polarization obtained from PUND data is seen to be decreasing toward lower temperatures [Fig. 2(b)], peaking at a temperature T_{rg} deviating from the trend in normal ferroelectrics. It is also observed that this value of T_{rg} is electric-field-dependent (not shown here), and at higher fields the trend follows that of normal ferroelectrics. These results suggest that the system transforms into a metastable FE state at low temperature and can be stabilized into a FE state with the application of high electric fields. Field-cooling protocols were adopted in earlier studies to probe the metastable nature of this system [11]. The coercive switching fields are also seen to be increasing below T_{rg}, as seen from hysteresis curves in Fig. 2. Our results are strikingly similar to the dielectric and electric polarization studies in the $(Ba_{0.925}Bi_{0.05})(Ti_{1-x}Sn_x)O_3$ system, where a reentrant transition from a ferroelectric to a glasslike state is observed [28] from transmission electron microscopy measurements. Adopting similar nomenclature to that used in the literature, this characteristic temperature T_{rg} is taken as the reentrant temperature. However, with further analysis we establish the true nature associated with this temperature.

Further, the electric polarization trend with electric fields obtained from hysteresis curves taken at different temperatures is studied to realize the nature of this reentrant state, and the data are shown in Fig. 3. The trend obtained follows the polynomial that is adopted for relaxor studies [33], as shown in the inset of Fig. 3(a). And the derivative [as also shown in Fig. 3(b)] that corresponds to the static dielectric constant is plotted against electric field. The derivative, which shows a maximum, corresponds to the transformation from the relaxor ferroelectric state to the long-range ferroelectric state [33]. It was also conjectured by Sanjay *et al.* [11] that this system coexists in ferroelectric and relaxor states towards low temperatures. The results of electric polarization with an electric field and Vogel-Fulcher-like dielectric dispersion points towards the relaxorlike signature. These results led us to believe that the metastable nature of this system is given by the relaxor-like properties that are observed. To further understand the evolution of electric polarization in such systems, first-order reversal curves are measured and subsequently analyzed as discussed in the following section.

B. First-order reversal curves

First-order reversal curves $P(E_r, E)$ [34] have been measured at selected temperatures, starting from room temperature [Fig. 4(a)]. Each curve is preceded by a preparation step,

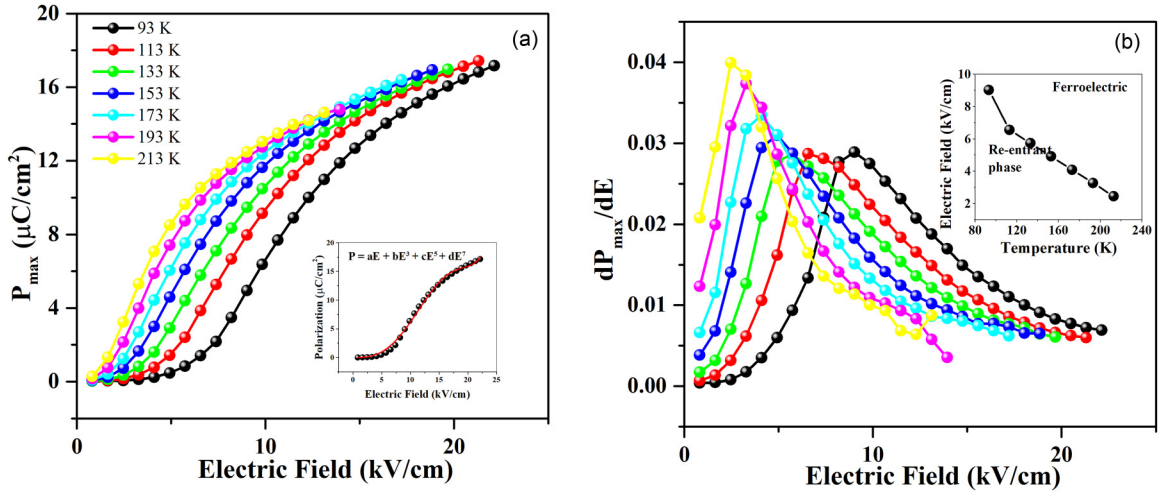

FIG. 3. (a) Maximum electric polarization (P_{max}) plotted as a function of electric field, taken from the temperature-dependent *P-E* data. The inset shows polynomial fitting for 80 K as adopted in the literature [33]. (b) Its derivative and the inset show the electric field corresponding to derivative maxima against the temperature.

where the applied field is decreased from positive saturation to the so-called reversal field E_r, and it consists in measurements of P while the applied field E is increased from E_r to positive saturation. The FORC function $\rho = \partial^2 P/(\partial E_r \partial E)$ has been calculated with the VARIFORC protocol using local polynomial fits [35], and plotted in modified coordinates $E_c = (E - E_r)/2$ and $E_b = (E + E_r)/2$ [Fig. 4(b)]. In Preisach theory [34], E_c and E_b are the coercive and bias fields of elemental rectangular hysteresis loops, called hysterons, and the FORC function is the joined probability density of these fields, which is required to generate the measured curves. The room-temperature (∼293 K) FORC function is concentrated along the left margin ($E_c = 0$) and has a large vertical spread with a single maximum close to the origin. This signature is typical of a system containing regions whose remanent polarization $P(E = 0)$ decays in a time comparable with that of the measurements, due to thermal relaxation [36]. The hysteresis becomes completely closed above T_C, yielding $\rho = 0$. The approach to T_C is clearly visible in the temperature dependence of the remanent saturation polarization $P_{rs} = P(E_r, E = 0)$ and of the total irreversible polarization P_{FORC} obtained by integrating the FORC function over E_c and E_b (Table I). Both quantities disappear at $T_C \approx 297$ K [Fig. 5(a)], in correspondence with the peak of the dielectric constant (Fig. 2). For comparison, the saturation polarization P_s displays only a moderate decrease in proximity to T_C.

Isolated regions undergoing thermal relaxation near T_C produce FORC functions characterized by a vertical ridge at $E_c = 0$, which extends mainly over $E_b \lesssim 0$, since a negative reversal field is required to switch these regions [36]. In the formalism of the Preisach theory, the almost symmetric ridge observed at room temperature requires a random bias field E_b with a broad probability distribution, which acts as a thermal fluctuation field with spatial and time correlation [37]. The existence of a strong random coupling between relaxing regions is also suggested by the amplitude-dependent, frequency-independent maximum of tanδ in measurements of the dielectric constant around ∼290 K (Fig. 2), which contrasts with the amplitude-independent and frequency-independent behavior expected from thermal relaxations in noninteracting systems [38].

A second FORC feature emerges at lower temperatures. This feature consists of a second peak, hereafter called the central peak, which forms near the origin [Fig. 4(b), 273 K] and moves towards higher values of E_c as the temperature decreases. A similar feature, consisting of a horizontal ridge along $E_b = 0$, is produced by the switching of isolated regions that become progressively blocked [36]; however, the central maximum seen here is characterized by oval contour lines, which, as in the case of the vertical ridge caused by thermal relaxation, denote the presence of random interactions [39]. In the context of Preisach theory, such interactions are represented by a local internal field whose probability distribution density is given by vertical profiles through the FORC function [34,40]. The central peak is offset toward negative E_b values comprised between ∼0.2 kV/cm (273 K) and ∼1.2 kV/cm (123 K), which can be understood as a positive mean internal field that promotes switching to positive saturation in external fields that are smaller than those required without this internal field. A pair of positive and negative ridges parallel to the descending diagonal departs from the central peak, while the vertical ridge near the left edge of the FORC diagram is shifted downwards. Similar signatures have been observed in polycrystalline exchange-spring magnets consisting of a magnetically hard/soft bilayer [41], and in polycrystalline iron thin films [42]. The development of the diagonal ridge pair has also been associated with the formation of long-range ferromagnetic order between ferromagnetic clusters embedded in a nonferromagnetic matrix [43].

Ferroelectric exchange coupling can be represented by a so-called exchange electric field $E_{ex} = \alpha P$ that is proportional to the bulk polarization through a positive coefficient α. In this case, switching of ferroelectric regions depends on the total field $E_{tot} = E + \alpha P$ resulting from the overlap of E_{ex} with the field E applied during FORC measurements. Electric polarization curves expressed as a function of E_{tot}, instead of the applied field, represent the intrinsic response of the switching regions without any coupling between them. This operation is

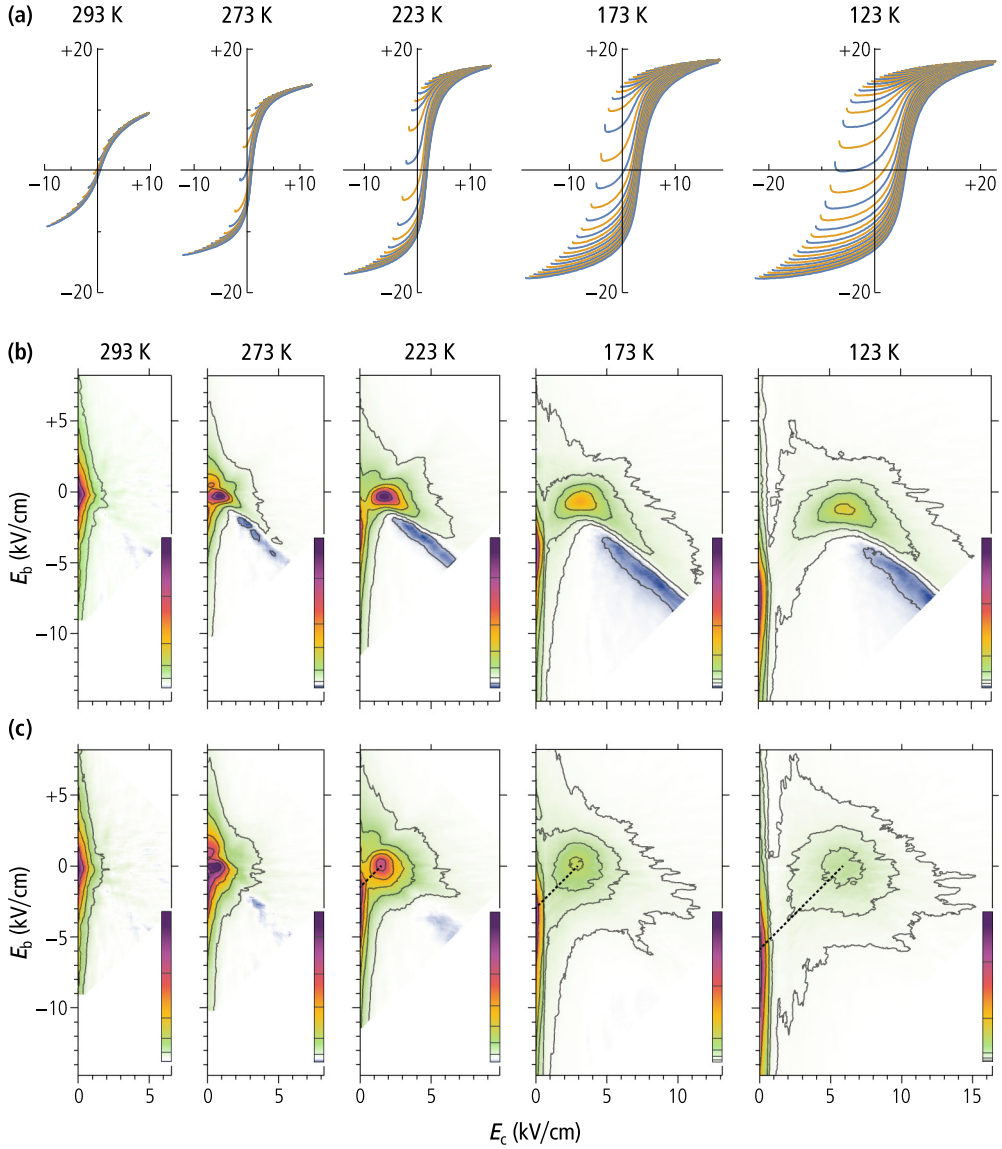

FIG. 4. (a) FORC measurements at 293, 273, 223, 173, and 123 K (every fifth curve is shown for clarity, electric field in kV/cm along x-axis, and polarization in μC/cm^2 along y-axis. (b) FORC diagrams corresponding to the measurements in (a). Contours enclose polarizations corresponding to the 15%, 40%, 60%, and 80% quantiles of the total integral of the FORC function. (c) FORC diagrams corresponding to the measurements in (a), expressed as a function of the total internal field $E_i = E + \alpha P/\epsilon_0$, instead of the applied field E, with coefficients α given in Table I. The dashed lines connect the peaks of the thermal relaxation feature on the left margin with the central maximum along the trace of a single curve.

called deshearing [34]. If FE exchange is representable by the above model, a value of α can be found for which the diagonal ridge pair is eliminated from the desheared FORC diagram, while the central maximum moves to the $E_b = 0$ position expected for unbiased switching regions. This is indeed the case [Fig. 4(c)], with increasingly large values of α required at lower temperatures (Table I). Hysteresis deshearing with $\alpha > 0$ causes a decrease of P_{rs}, whereby $P_{rs}/P_s \approx 0.5$ is obtained from desheared P_{rs} values at low temperatures. This result is expected for isolated and completely blocked regions with uniaxial ferroelectric anisotropy.

The amplitude of the central maximum in desheared FORC diagrams decreases with decreasing temperature; however, this is just due to its broadening, since P_{FORC} increases monotonically as the sample is cooled down (Fig. 5). The median $\langle E_c \rangle$ of the distribution obtained from horizontal profiles of the FORC function (Table I) is a measure for the mean switching field. It is characterized by a strong temperature dependence, and it vanishes near T_C because of thermal relaxations. The vertical extension of the desheared central maximum is a measure for the strength of random interactions between switching regions, expressed, for instance, by the standard deviation $\sigma(E_b)$ of a probability density function identified by vertical profiles across the central maximum. Estimates of $\sigma(E_b)$ have been obtained for $T \leqslant 223$ K (Table I); above this temperature, the central maximum overlaps with the vertical ridge caused by thermal relaxation, yielding unreliable results. The similarity between the magnitude and the temperature

TABLE I. Parameters derived from FORC measurements: P_s, saturation polarization; P_{rs}, remanent saturation polarization; P_{rsd}, remanent saturation polarization obtained from desheared measurements; P_{forc}, integral of the FORC function over the measured domain; $\langle E_c \rangle$, median switching field calculated from horizontal profiles of the desheared FORC function at $E_b = 0$ and over $E_c \geqslant 0.6$ kV/cm (to exclude contributions from the vertical ridge); α, deshearing coefficient; $\sigma(E_b)$, standard deviation of the distribution of bias fields obtained from vertical profiles of the desheared FORC function through the central maximum; $E_{ex} = \alpha P$, mean exchange field. An asterisk indicates not determined because of the overlap with the vertical ridge.

T (K)	P_s (μC/cm^2)	P_{rs} (μC/cm^2)	P_{rsd} (μC/cm^2)	P_{forc} (μC/cm^2)	P_{rsd}/P_{forc}	$\langle E_c \rangle$ (kV/cm)	α (kV/cm)	$\sigma(E_b)$ (kV/cm)	E_{ex} (kV/cm)
293	14.5	1.26	1.05	1.69	0.073	0.43	~820	*	1.19
273	16.3	6.16	4.28	6.72	0.26	0.76	~820	*	1.34
223	19.1	10.5	8.78	12.9	0.46	1.73	820	1.62	1.56
173	21.0	12.2	10.3	14.6	0.49	3.07	1150	2.19	2.41
123	21.3	13	11.3	15.2	0.53	5.83	1640	2.59	3.49

dependence of E_{ex} and $\sigma(E_b)$ [Fig. 5(b)] points to a common origin of these two quantities, which can be understood as the mean and the standard deviation of a positive random variate describing the intensity of local ferroelectric exchanges. As in the case of thermal relaxation near ~220 K, the presence of an interaction field is confirmed by the frequency-dependent amplitude maximum of tanδ in measurements of the dielectric constant in the reentrant spin-glass range [Fig. 2(a)].

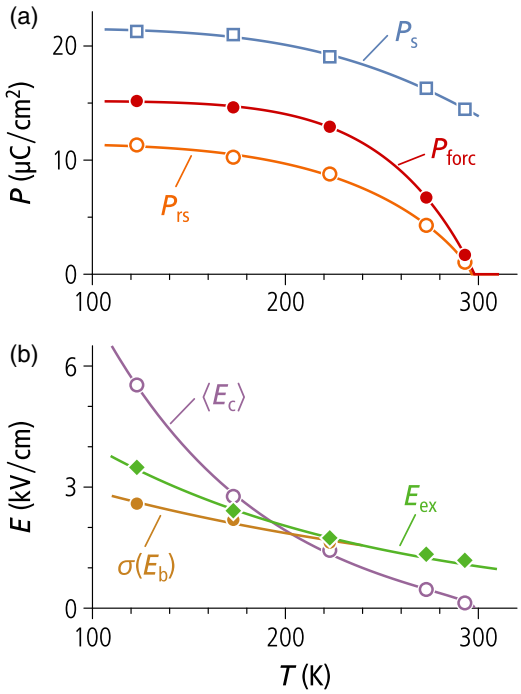

FIG. 5. (a) Saturation polarization P_s (squares), remanent saturation polarization P_{rs}, and total FORC polarization P_{forc} (dots) obtained from the desheared FORC measurements shown in Fig. 4. Lines are guides to the eye. (b) Temperature dependencies of the exchange field E_{ex} (diamonds), the median switching field $\langle E_c \rangle$ (circles), defined as the median of the coercivity distribution represented by horizontal profiles of the FORC functions in Fig. 4(c) at $E_b = 0$, and the standard deviation of the random bias field E_b (dots), obtained from vertical profiles of the FORC function in Fig. 4(c) across the central maximum. Lines are guides to the eye.

Further, the peak of the thermal relaxation feature along the left edge of the desheared FORC diagrams is connected to the central maximum by a 45° line [dotted in Fig. 4(c)], which means that curves with the most switching are also those affected by the largest relaxation effects associated with the hook-shaped initial part [Fig. 4(a)]. As mentioned above, the initial polarization decrease can be explained by the thermally activated switching of positively saturated regions in proximity to the negative reversal field [36]. The same regions are switched back to positive saturation, in agreement with the central maximum of the FORC diagram.

Further, to demonstrate the structural changes that are associated with the electric polarization evolution, spectroscopic techniques viz., Mössbauer, Raman, and XANES, are employed and are discussed in the following sections.

C. Raman spectroscopy investigation

Room-temperature Raman spectroscopy as shown in Fig. 6 shows modes resembling rhombohedral/orthorhombic/tetragonal modes that are symmetry-forbidden for the $Pm\bar{3}m$ space group, as evidenced from XRD of the same sample (Fig. 1). This is a consequence of the local structure deviating from the average structure, which is common in materials exhibiting DPT [29]. However, due to broad overlapping modes, it is nearly impossible to distinguish the exact local structure

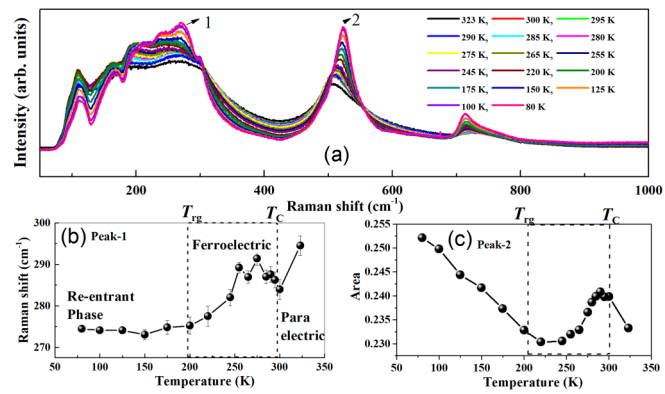

FIG. 6. (a) Representative temperature-dependent Raman spectra of $BaSn_{0.15}Ti_{0.85}O_3$. Temperature variation of (b) Raman shift of peak-1 and (c) normalized area of peak-2.

near room temperature. It can still be seen from the spectra taken at 323 K ($>T_C$) that modes still persist indicating that local structure is preserved well above T_C. This is generally observed in DPT where it is suspected that nucleation of the low-temperature phase starts appearing at very high temperatures ($>T_C$).

Despite the abrupt changes in wave number that are seen around this temperature range (T_C), more temperature points above T_C are needed to conclude the phase transition as observed from Raman spectroscopy. It is expected that in DPT the changes in local structure associated with phase transition are reflected at higher temperatures than the T_C observed from dielectric measurements. However, this paper focuses on explaining the low-temperature peculiar behavior as observed from dielectric and electric polarization data, hence the spectroscopy analysis is limited to temperatures below T_C.

The temperature-dependent evolution of the A(TO) mode wave number corresponding to octahedral vibrations against a barium atom is show in Fig. 6(b). This mode is susceptible to phase transitions in pure BTO showing discontinuous jumps across different phase transitions, viz., cubic-tetragonal-orthorhombic-rhombohedral [44]. The wave number of this mode shows a sharp decrease upon lowering temperatures near the phase transitions. Similarly, a decrease in wave number is observed in the present work, albeit gradually as a consequence of the diffuse nature of the phase transition. These results suggest that the system transforms to rhombohedral [11] in a wide temperature range, as expected for DPT systems. Further, the area under the polar TO mode is calculated ($\approx$535 cm^{-1}), and it is seen to be decreasing below T_C and increasing toward low temperatures. All the spectra are corrected with the Bose-Einstein factor before calculating the area of the TO mode to eliminate the varying population contribution with temperature [45]. The structural inhomogeneity in the compounds showing DPT is well known, and thus this decrease can be attributed to the system transforming to the much more ordered state by the interplay between the increasing ferroelectric and decreasing paraelectric nature present in the system even below T_C. These results, along with the wave-number trend with temperature, emphasize the DPT nature present in the system. However, an unusual increase in area is observed towards low temperatures ($<T_{rg}$). Such an increase might likely be due to the increase in structural disorder, for reasons that will be discussed in the next sections. The Mössbauer technique is further employed to complement these results, which are discussed in the next section.

D. Mössbauer analysis

Mössbauer spectra taken at different temperatures between 100 and 300 K are shown in Fig. 7. The width obtained from the spectral fitting against the temperature is also shown in the same figure. The Mössbauer spectral width, which is proportional to the electric field gradient, gives information about the local environment around the Sn nucleus. The usual trend in ferroelectrics follows an increasing value of width below the Curie temperature as a consequence of polar ordering giving rise to a nonsymmetrical environment around the Sn nucleus. However, below T_C an anomalous trend is observed here where decreasing width is observed upon lowering the temperature, contrary to the observed increase in ferroelectric transitions [14]. The reason for such an observation is similar to the one discussed earlier, and it can be explained within the context of the interplay between paraelectric and ferroelectric relative phase fractions, which would result in such a decrease in linewidth below T_C. Upon further lowering the temperature, an increasing trend in width is observed below T_{rg}, complemented again by Raman results, viz., an onset of disorder in the system. Such an increase in width also resembles the increasing width across the relaxor transition in relaxors [29], thereby correlating the dispersion trend observed in the dielectric data.

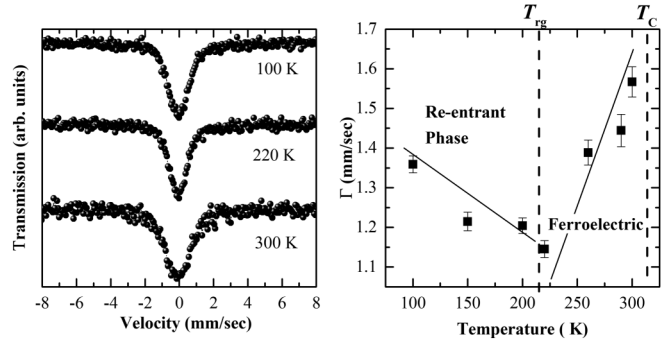

FIG. 7. Left: Representative temperature-dependent ^{119}Sn Mössbauer spectra of $BaSn_{0.15}Ti_{0.85}O_3$. Right: Temperature variation of the width of ^{119}Sn Mössbauer, considered to be proportional to the electric field gradient.

E. Ti *K*-edge x-ray absorption spectroscopy investigation

X-ray near-edge spectroscopy (XANES) performed near the Ti-*K* edge at various temperatures is presented in Fig. 8. The inset shows the preedge region with the peaks labeled as *a*, *b*, *c*, and *c*′. The details corresponding to the origin of these peaks are widely discussed in the literature [29]. In particular, with regard to the behavior of peak *b*, its intensity with temperature reveals information about TiO_6 distortions. In fact, it corresponds to electronic excitation to empty Ti *d* states below the continuum, having a quadrupolar transition rule. The *p*-*d* hybridization with oxygen levels enhances the dipole-allowed transition probability. Such hybridization is forbidden in a regular TiO_6 octahedron but increases for distorted octahedra and/or off-center Ti displacement [46]. And it is demonstrated that across the phase transitions in BTO, the octahedra are susceptible to distortions, reflected in the changes in peak position and the intensity of peak *b* [47]. The preedge features were analyzed as a combination of Gaussian peaks. The intensity of the peak *b* is plotted against the temperature in Fig. 8, and it is evident that two different regions exist below T_C, separated by dashed lines in Fig. 8, showing different behavior in intensity of peak *b* with temperature. In particular, upon lowering the temperature below T_{rg}, the peak *b* rises. This shows that with the occurrence of TiO_6 octahedral distortions, such off-center Ti displacement allows the FE order to be established. Below T_{rg}, a different slope of the *b* peak with respect to temperature change is evident, suggesting a different behavior that may originate from establishing local

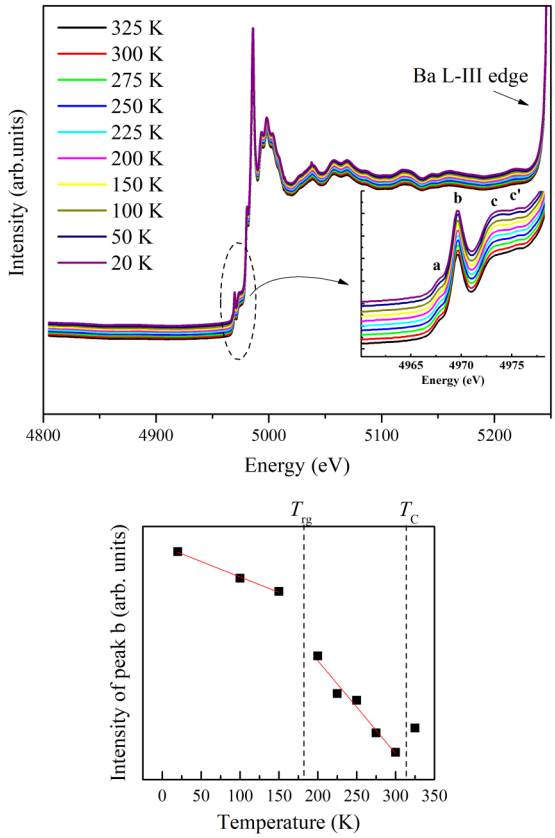

FIG. 8. Top: Representative temperature-dependent x-ray absorption spectra (XAS) of $BaSn_{0.15}Ti_{0.85}O_3$. The data are vertically shifted. Inset shows the representative fitting of different modes in the preedge region for 300 K data. Bottom: Variation of the integral area of peak-b with temperature.

inhomogeneities related to polar nanoregions in the relaxor phase.

IV. SUMMARY AND CONCLUSIONS

In summary, we studied the diffuse phase transition occurring in $BaSn_{0.15}Ti_{0.85}O_3$. The dielectric data confirm the system's paraelectric-ferroelectric transformation over a broad range of temperature, a characteristic of DPT. Within this region, spatial inhomogeneities in structure, viz., coexisting in different phases, are confirmed from the trends in Mössbauer and Raman spectral analysis. The remanent polarization obtained from *P-E* hysteresis loops is seen increasing on cooling till T_{rg}, correlating with the trend observed in ferroelectrics. Below T_{rg}, the remanent polarization starts to decrease, and concomitantly a significant dielectric dispersion becomes evident. This low-temperature phase ($<T_{rg}$) is denoted as a reentrant phase with relaxorlike properties, in agreement with the literature, viz., Vogel-Fulcher-like dispersion in the dielectric loss, a decrease in remanent polarization, and the trend in maximum polarization with electric field. The increasing linewidths and the area of Mössbauer spectra and Raman spectroscopy at low temperatures upon cooling further signal a much disordered state at low temperatures.

Further, the polarization evolution with temperature is studied from the FORC distribution. The FORC distribution reveals that clusters with ferroelectric ordering start to form within the range of Curie temperatures. A similar phenomenon is described by Davies *et al.* [43], who call it an "isolated clusters phase." If really isolated, they produce a FORC signature consisting of a vertical ridge along the left edge of the FORC space, entirely confined in the lower quadrant [36]. In reality, we see a ridge that extends symmetrically in the upper and lower quadrants, and this can only be explained by the presence of a random bias field originating from interactions between these regions. So, these are definitively not isolated regions. Also, unlike in Ref. [43], ordering starts in a blocking state, as shown by their FORC diagram, while we start in an unblocked state, where the polarization of ordered regions decays in time. The room-temperature FORC diagram thus shows that ordering does not start at the level of single, totally isolated crystals, as one might expect from compositional variations. Instead, a sort of loose network with FE ordering is forming (maybe along grain boundaries).

The FORC studies do not reveal any thermodynamic phase transition near T_{rg}. Instead, it is seen that the ferroelectric exchange field that represents the interaction strength between different regions in the sample is increasing with temperature. This behavior suggests no breaking of long-range order in the system at low temperatures, and the ferroelectric nature is increasing at all temperatures. On the other hand, the regions that are susceptible to fluctuations with temperature are observed at all measured temperatures, viz., relaxorlike entities that exist at all temperatures. The FORC analysis after deshearing points to the existence of regions that are subjected to both thermal relaxation and exchange interactions.

One must note that multidomain (MD) and relaxor processes can produce a similar FORC signature consisting of a vertical ridge at $E_c = 0$. In the MD case, this is caused by individual curves being flat in proximity to the reversal field (E_r), because of domain pinning [48]. However, in our case, the vertical ridge is caused by "hook-shaped" curves, characterized by an initial decrease of the polarization for applied field values close to E_r (Fig. 4). This decrease, which depends also on the timing of the measurements, is a characteristic of viscous systems [48], and it reveals the relaxation nature of this feature.

In conclusion, the FORC analysis provides a picture of polar regions that switch as expected from an ideal single-domain behavior, but the switching field depends on time: the more time that is spent at a certain field, the more likely it is that some particles will be switched. Contrary to magnetic nanoparticle systems, the regions are affected by exchange coupling, probably across the grain boundaries. Cooling below 100 K is expected to progressively block the entire specimen volume, and it produces the decrease of tanδ seen in Fig. 2. A very noticeable result is that the ratio between saturation remanent polarization and saturation polarization approaches 0.5 if calculated from desheared data, that is, as if the regions were uncoupled. This ratio is expected for randomly oriented domains with uniaxial anisotropy. Such randomness of anisotropies in the system might result either from the microstructure of the polycrystalline or from having to contain local heterogeneities of different polar

symmetries from its macroscopic structure. The latter reason might explain the increasing linewidths of Raman and Mössbauer spectra, XANES anomalies at low temperatures, and also the increase in the random component of the exchange field [$\sigma(E_b)$], as different local polar orders percolate in the measured temperature range. Fang *et al.* [28] obtained similar FORC results on barium-titanate-based systems, which they could link by imaging techniques to reentrant glass behavior with different coexisting anisotropies. Hence the reentrant behavior we observed is a heterogeneous system with macroscopic disorder that behaves like a glass, rather than being a proper spin glass. In conclusion, FORC appears to be a suitable technique for investigating low-temperature relaxor behavior governed by exchange interactions, which can contribute to a better understanding of relaxor compositions and other known materials with reentrant characteristics.

ACKNOWLEDGMENTS

A.S. and V.R.R. thank Department of Science and Technology (DST) and IISc, Bangalore for travel support for performing experiments at XAFS beamline, ELETTRA. Authors thank V. G. Sathe for the Raman spectroscopy measurements. Thanks are due to Giuliana Aquilanti and Luca Olivi for the help during XAFS measurements at Elettra. Mr. Anil Gome is acknowledged for the help with Mössbauer spectroscopy measurements.

[1] V. Isupov, Some problems of diffuse ferroelectric phase transitions, Ferroelectrics **90**, 113 (1989).

[2] V. Isupov, Phenomena at transformation from sharp to diffuse ferroelectric phase transition, Ferroelectrics **143**, 109 (1993).

[3] G. Smolensky, V. Bokov, V. Isupov, N. Krainik, R. Pasynkov, and A. Sokolov, *Ferroelectrics and Related Materials* (Gordon and Breach, Switzerland, 1984).

[4] N. Setter and L. Cross, The contribution of structural disorder to diffuse phase transitions in ferroelectrics, J. Mater. Sci. **15**, 2478 (1980).

[5] T. Tsurumi, K. Soejima, T. Kamiya, and M. Daimon, Mechanism of diffuse phase transition in relaxor ferroelectrics, Jpn. J. Appl. Phys. **33**, 1959 (1994).

[6] R. Pirc, Z. Kutnjak, and N. Novak, Compressible spherical dipolar glass model of relaxor ferroelectrics, J. Appl. Phys. **112**, 114122 (2012).

[7] R. Pirc, R. Blinc, and Z. Kutnjak, Nonlinear dielectric response of relaxor ferroelectrics, Phys. Rev. B **65**, 214101 (2002).

[8] M. Tyunina and J. Levoska, Effect of ac field on the dielectric behavior in epitaxial films of relaxor ferroelectric $PbMg_{1/3}Nb_{2/3}O_3$, Phys. Rev. B **72**, 104112 (2005).

[9] Z.-R. Liu, B.-L. Gu, and X.-W. Zhang, Effects of ac field amplitude on the dielectric susceptibility of relaxors, Phys. Rev. B **62**, 1 (2000).

[10] D. Fu, H. Taniguchi, M. Itoh, S.-y. Koshihara, N. Yamamoto, and S. Mori, Relaxor $PbMg_{1/3}Nb_{2/3}O_3$: A Ferroelectric with Multiple Inhomogeneities, Phys. Rev. Lett. **103**, 207601 (2009).

[11] S. K. Upadhyay, V. R. Reddy, S. Gupta, N. Lalla, and K. Singh, Co-existence of ferroelectric and relaxor phase in polycrystalline Sn doped $BaTiO_3$ and tuning their phase fraction with electric field, Solid State Commun. **255**, 42 (2017).

[12] V. Shvartsman, J. Dec, Z. Xu, J. Banys, P. Keburis, and W. Kleemann, Crossover from ferroelectric to relaxor behavior in $BaTi_{1-x}Sn_xO_3$ solid solutions, Phase Trans. **81**, 1013 (2008).

[13] V. Shvartsman, J. Zhai, and W. Kleemann, The dielectric relaxation in solid solutions $BaTi_{1-x}Zr_xO_3$, Ferroelectrics **379**, 77 (2009).

[14] S. K. Upadhyay, V. R. Reddy, P. Bag, R. Rawat, S. Gupta, and A. Gupta, Electro-caloric effect in lead-free Sn doped $BaTiO_3$ ceramics at room temperature and low applied fields, Appl. Phys. Lett. **105**, 112907 (2014).

[15] N. Yasuda, H. Ohwa, and S. Asano, Dielectric properties and phase transitions of $Ba(Ti_{1-x}Sn_x)O_3$ solid solution, Jpn. J. Appl. Phys. **35**, 5099 (1996).

[16] C. Lei, A. A. Bokov, and Z.-G. Ye, Ferroelectric to relaxor crossover and dielectric phase diagram in the $BaTiO_3$-$BaSnO_3$ system, J. Appl. Phys. **101**, 084105 (2007).

[17] M. A. Ansari and K. Sreenivas, Effects of disorder activated scattering and defect-induced phase on the ferroelectric properties of $BaSn_xTi_{1-x}O_3 (0 \leqslant x \leqslant 0.28)$ ceramics, Ceram. Int. **45**, 20738 (2019).

[18] T. Shi, L. Xie, L. Gu, and J. Zhu, Why Sn doping significantly enhances the dielectric properties of $Ba(Ti_{1-x}Sn_x)O_3$, Sci. Rep. **5**, 8606 (2015).

[19] L. Xie, Y. L. Li, R. Yu, Z. Y. Cheng, X. Y. Wei, X. Yao, C. L. Jia, K. Urban, A. A. Bokov, Z.-G. Ye *et al.*, Static and dynamic polar nanoregions in relaxor ferroelectric $Ba(Ti_{1-x}Sn_x)O_3$ system at high temperature, Phys. Rev. B **85**, 014118 (2012).

[20] M. Deluca, L. Stoleriu, L. P. Curecheriu, N. Horchidan, A. C. Ianculescu, C. Galassi, and L. Mitoseriu, High-field dielectric properties and raman spectroscopic investigation of the ferroelectric-to-relaxor crossover in $BaSn_xTi_{1-x}O_3$ ceramics, J. Appl. Phys. **111**, 084102 (2012).

[21] S. Senoussi, S. Hadjoudj, and R. Fourmeaux, Magnetic Structures in Reentrant Spin-Glasses Observed by Transmission Electron Microscopy, Phys. Rev. Lett. **61**, 1013 (1988).

[22] T. Sato, T. Ando, T. Ogawa, S. Morimoto, and A. Ito, Spin freezing and the ferromagnetic and reentrant spin-glass phases in a reentrant ferromagnet, Phys. Rev. B **64**, 184432 (2001).

[23] J. Dho, W. S. Kim, and N. H. Hur, Reentrant Spin Glass Behavior in Cr-Doped Perovskite Manganite, Phys. Rev. Lett. **89**, 027202 (2002).

[24] A. A. Bokov and Z.-G. Ye, Reentrant phenomena in relaxors, in *Nanoscale Ferroelectrics and Multiferroics: Key Processing and Characterization Issues, and Nanoscale Effects* (ResearchGate, 2016), Vol. 1, p. 729.

[25] S. S. N. Bharadwaja, J. R. Kim, H. Ogihara, L. E. Cross, S. Trolier-McKinstry, and C. A. Randall, Critical slowing down mechanism and reentrant dipole glass phenomena in $(1\text{-}x)BaTiO_3$-$xBiScO_3 (0.1 \leqslant x \leqslant 0.4)$: The high energy density dielectrics, Phys. Rev. B **83**, 024106 (2011).

[26] K. Li, X. Li Zhu, X. Qiang Liu, and X. Ming Chen, Re-entrant relaxor behavior of $Ba_5RTi_3Bb_7O_{30}$ (R= La, Nd, Sm) tungsten bronze ceramics, Appl. Phys. Lett. **102**, 112912 (2013).

[27] S. Bharadwaja, S. Trolier-McKinstry, L. Cross, and C. A. Randall, Reentrant dipole glass properties in (1-x)$BaTiO_3$-x$BiScO_3$, $0.1 \leqslant x \leqslant 0.4$, Appl. Phys. Lett. **100**, 022906 (2012).

[28] M. Fang, Y. Ji, Z. Zhang, Y. Yang, C. Liu, D. Wang, L. Zhang, J. Gao, and X. Ren, Re-entrant relaxor–ferroelectric composite showing exceptional electromechanical properties, NPG Asia Mater. **10**, 1029 (2018).

[29] A. Surampalli, I. Schiesaro, P. Corsi, C. Meneghini, V. G. Sathe, A. Sagdeo, A. K. Sinha, G. Aquilanti, E. Welter, and V. R. Reddy, Evidence of structural modifications in the region around the broad dielectric maxima in the 30% Sn-doped barium titanate relaxor, Phys. Rev. B **100**, 134104 (2019).

[30] A. D. Cicco, G. Aquilanti, M. Minicucci, E. Principi, N. Novello, A. Cognigni, and L. Olivi, Novel XAFS capabilities at ELETTRA synchrotron light source, J. Phys.: Conf. Ser. **190**, 012043 (2009).

[31] C. Meneghini, F. Bardelli, and S. Mobilio, Estra-fitexa: A software package for EXAFS data analysis, Nuclear Instr. Methods Phys. Research Sec. B: Beam Inter. Mater. Atoms **285**, 153 (2012).

[32] J. Rodríguez-Carvajal, Recent advances in magnetic structure determination by neutron powder diffraction, Phys. B: Condens. Matter **192**, 55 (1993).

[33] S. Prosandeev, D. Wang, A. R. Akbarzadeh, B. Dkhil, and L. Bellaiche, Field-Induced Percolation of Polar Nanoregions in Relaxor Ferroelectrics, Phys. Rev. Lett. **110**, 207601 (2013).

[34] R. Egli, Magnetic characterization of geologic materials with first-order reversal-curves, in *Magnetic Measurement Techniques for Materials Characterization*, edited by J. V. Franco and B. Dodrill (Springer International Publishing, Cham, 2021), pp. 455–604.

[35] R. Egli, Variforc: An optimized protocol for calculating non-regular first-order reversal curve (forc) diagrams, Glob. Planet. Change **110**, 302 (2013).

[36] L. Lanci and D. V. Kent, Forward modeling of thermally activated single-domain magnetic particles applied to first-order reversal curves, J. Geophys. Res.: Solid Earth **123**, 3287 (2018).

[37] D. Berkov and N. Gorn, Micromagnetic simulations using langevin dynamics studying thermal field correlations, J. Magn. Magn. Mater. **272**, 687 (2004).

[38] P. E. Jonsson, Superparamagnetism and spin glass dynamics of interacting magnetic nanoparticle systems, Adv. Chem. Phys. **128**, 191 (2004).

[39] C. Carvallo, D. J. Dunlop, and Ö. Özdemir, Experimental comparison of forc and remanent preisach diagrams, Geophys. J. Int. **162**, 747 (2005).

[40] R. Egli, Theoretical considerations on the anhysteretic remanent magnetization of interacting particles with uniaxial anisotropy, J. Geophys. Res.: Solid Earth **111**, B12S18 (2006).

[41] J. E. Davies, O. Hellwig, E. E. Fullerton, J. Jiang, S. Bader, G. Zimanyi, and K. Liu, Anisotropy dependence of irreversible switching in Fe/ SmCo and FeNi/ FePt exchange spring magnet films, Appl. Phys. Lett. **86**, 262503 (2005).

[42] Y. Cao, K. Xu, W. Jiang, T. Droubay, P. Ramuhalli, D. Edwards, B. R. Johnson, and J. McCloy, Hysteresis in single and polycrystalline iron thin films: Major and minor loops, first order reversal curves, and preisach modeling, J. Magn. Magn. Mater. **395**, 361 (2015).

[43] J. E. Davies, J. Wu, C. Leighton, and K. Liu, Magnetization reversal and nanoscopic magnetic-phase separation in $La_{1-x}Sr_xCoO_3$, Phys. Rev. B **72**, 134419 (2005).

[44] C. Perry and D. Hall, Temperature Dependence of the Raman Spectrum of $BaTiO_3$, Phys. Rev. Lett. **15**, 700 (1965).

[45] T. Hart, R. Aggarwal, and B. Lax, Temperature dependence of Raman scattering in silicon, Phys. Rev. B **1**, 638 (1970).

[46] J. Itie, B. Couzinet, A. Flank, P. Lagarde, and A. Polian, High pressure XAS at the Ti K edge on Titanate perovskites, in *X-Ray Absorption Fine Structure - XAFS13: 13th International Conference*, AIP Conf. Proc. No. 882 (American Institute of Physics, New York, 2007), pp. 241–243.

[47] B. Ravel, E. Stern, R. Vedrinskii, and V. Kraizman, Local structure and the phase transitions of $BaTiO_3$, Ferroelectrics **206**, 407 (1998).

[48] C. R. Pike, A. P. Roberts, and K. L. Verosub, First order reversal curve diagrams and thermal relaxation effects in magnetic particles, Geophys. J. Int. **145**, 721 (2001).